The universe traced by clusters

Yasushi Suto

Department of of Physics
Research Center for the Early Universe
The University of Tokyo, Japan

July 5, 2000 @ Institut d'Astrophysique de Paris

Contents

1 **Why clusters ?** **2**

2 **An incomplete list: cosmology with clusters** **3**

3 **SZ effect as a distance indicator** **4**

3.1 Sunyaev-Zel'dovich effect 4

3.2 Determining the distance and peculiar velocity 5

3.3 Reliabilities of the estimated H_0 and $v_{\rm pec}$ 7

4 **Cluster abundances** **9**

4.1 Predicting cluster abundances 10

4.2 Breaking the degeneracy 14

5 **Spatial correlation** **17**

6 **Universal density profile** **22**

6.1 Numerical results 23

6.2 Observational confrontation 28

6.3 Relation to nonlinear mass power spectrum 31

7 **Summary and conclusions** **32**

1 Why clusters ?

Large:

dynamical time-scale comparable to the age of the universe $\rightarrow$ retains the cosmological initial condition

Multi-band:

current and future observations in various bands:

optical survey: APM, 2dF, SDSS

X-ray: Einstein, ROSAT, ASCA
XMM-Newton, Chandra

SZ in cm, mm & submm:
BIMA, OVRO, SCUBA, PLANCK, LMSA

Gravitational lensing: HST, Subaru, $\cdots$

Simple:

dark matter + gas + galaxies

$\rightarrow$ theoretically well-defined and

relatively easy to describe compared with galaxies

Bright:

important cosmological probe of high-z universe

2 An incomplete list: cosmology with clusters

distance indicator: H_0, Ω_0, λ_0

Sunyaev & Zel'dovich (1972), Silk & White (1978), Inagaki, Suginohara + YS (1996), Kobayashi, Sasaki + YS (1996), Birkinshaw (1999)

peculiar velocity field: $v_{\rm pec}$

Sunyaev & Zel'dovich (1972), Rephaeli & Lahav (1991), Holzapfel et al. (1997), Yoshikawa, Itoh + YS (1998)

mass fluctuation amplitude: σ_8, Ω_0

Henry & Arnaud (1991), Blanchard & Silk (1991), White, Efstathiou & Frenk (1993), Eke, Cole & Frenk (1996), Viana & Liddle (1996), Barbosa, Bartlett & Blanchard (1996), Kitayama + YS (1997)

spatial clustering and its evolution: $\xi(r,z)$, $b(r,z)$

Bahcall & Soneira (1983), Klypin & Kopylov (1983), Bahcall (1988), Bahcall & West (1992), Bahcall & Cen (1993), Ueda, Itoh + YS (1993), Watanabe, Matsubara + YS (1994), Borgani et al. (1999), Moscardini et al. (1999), YS, Yamamoto, Kitayama & Jing (2000)

baryon fraction and dark matter: Ω_b, Ω_0

White & Frenk (1991), Fabian (1991), Makino + YS (1993), White et al. (1993)

CMB anisotropy through the SZ effect: $\delta T/T$

Cole & Kaiser (1988), Makino + YS (1993), Komatsu & Kitayama (1999)

universal density profile/nonlinear clustering: $\rho(r)$, $P(k)$

Navarro, Frenk, & White (1996, 1997), Fukushige & Makino (1997), Moore et al. (1998), Jing + YS (2000), Seljak (2000), Ma & Fry (2000)

3 SZ effect as a distance indicator

3.1 Sunyaev-Zel'dovich effect

Inverse Compton scattering of the CMB photon by the high temperature electron gas in clusters

$$\Delta I_\nu^{\rm thermalSZ} = y \frac{x^4 e^x}{(e^x-1)^2}\left(x \coth\frac{x}{2} - 4\right)$$

$$x \equiv \frac{h\nu}{kT_{\rm CMB}}, \quad y = \int \frac{kT_{cl}(l) n_e(l)}{m_e c^2}\sigma_{\rm T} dl$$

Negative source at $\lambda > 1.38$mm ($\nu < 218$GHz)
Positive source in submm band

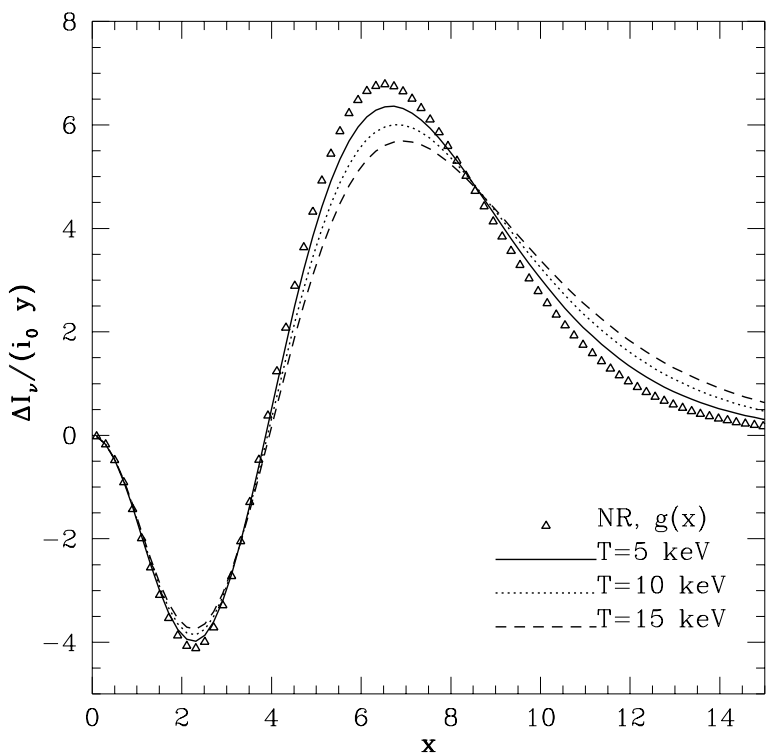

Figure 1: Spectral feature of the thermal Sunyaev-Zel'dovich flux. Independent of sources nor z.

3.2 Determining the distance and peculiar velocity

⋆ the angular diameter distance (H_0, Ω_0 & λ_0)

SZ temperature decrement: $\Delta T_{SZ} \propto R_{cl} T_{cl} n_e$

X-ray surface brightness: $S_X \propto R_{cl} T_{cl}^{1/2} n_e^2$

$$\Rightarrow R_{cl} \propto (\Delta T_{SZ})^2 / S_X$$

The proportional constant in the above expression can be specified if one neglects clumping, and adopt a spherical isothermal β-model with the observed X-ray temperature.

$$\rightarrow \quad d_A(z) = R_{cl}/\theta_{cl} = cz/H_0 \times [1 + O(z; \Omega_0, \lambda_0)]$$
$$\Rightarrow H_0, \Omega_0 \ \& \ \lambda_0$$

(e.g., Sunyaev & Zel'dovich 1972; Silk & White 1978; Birkinshaw, Hughes & Arnaud 1991; Rephaeli 1995; Kobayashi, Sasaki + YS 1996; Hughes & Birkinshaw 1998; Birkinshaw 1999)

⋆ peculiar velocity of clusters

Thermal and kinematic SZ fluxes have different frequency dependence $\Rightarrow$ cluster peculiar velocity

(e.g., Sunyaev & Zel'dovich 1980; Rephaeli & Lahav 1991; Holzapfel et al. 1997)

⋆ the Hubble diagram from the SZ effect

reasonable but not accurate enough (yet): $0.4 \lesssim h \lesssim 0.8$

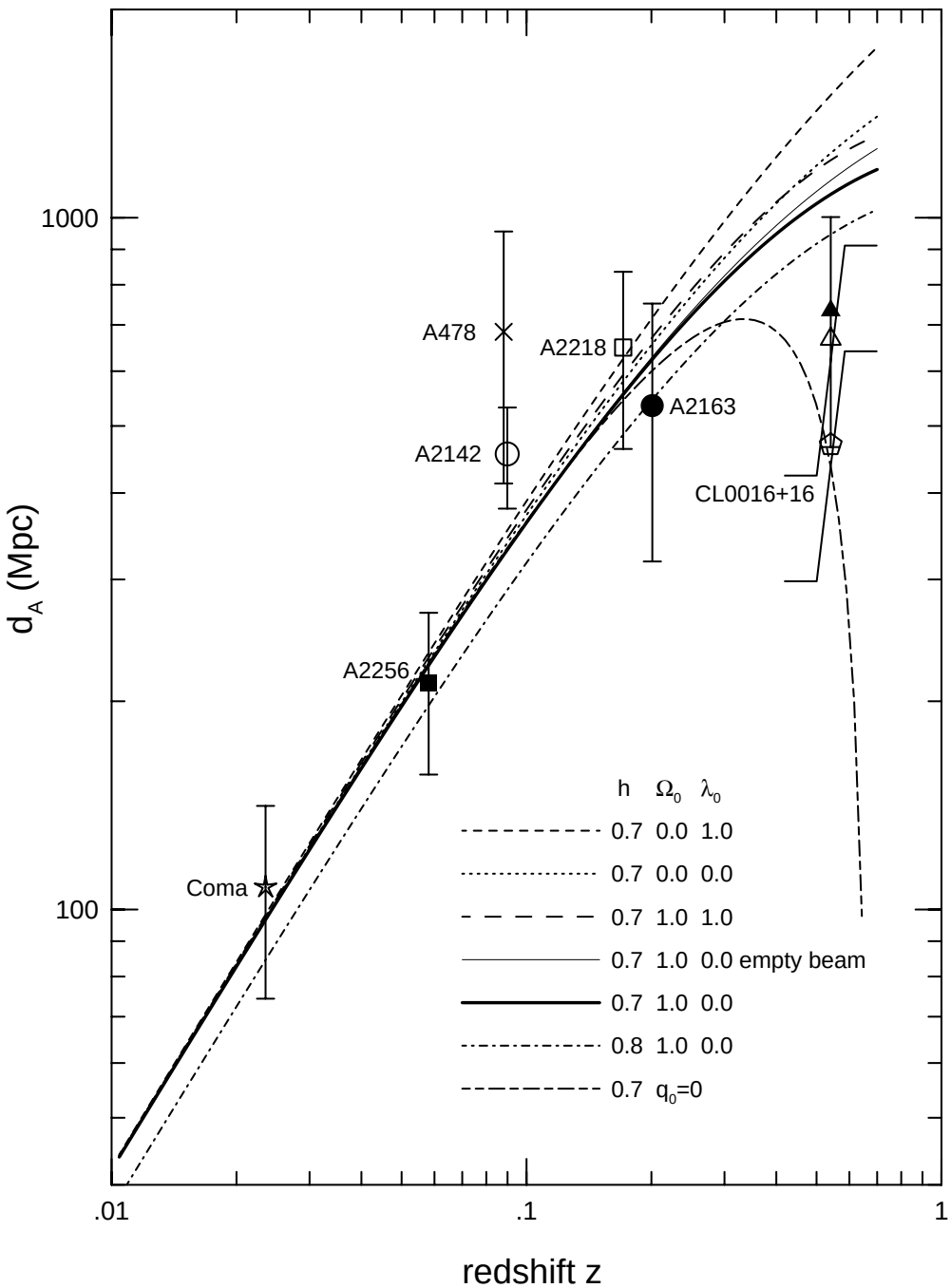

Figure 2: The angular diameter distances from the SZ effect. Kobayashi, Sasaki + YS PASJ **48**(1996)L107

3.3 Reliabilities of the estimated H_0 and $v_{\rm pec}$

Departure from the isothermal β-model (non-sphericity, substructure, non-isothermality, etc.) should produce different projection effects:

$\Downarrow$

Examine the reliabilities of the estimates of H_0 and peculiar velocities using numerical simulations (Inagaki, Suginohara + YS 1995; Yoshikawa, Itoh + YS 1998)

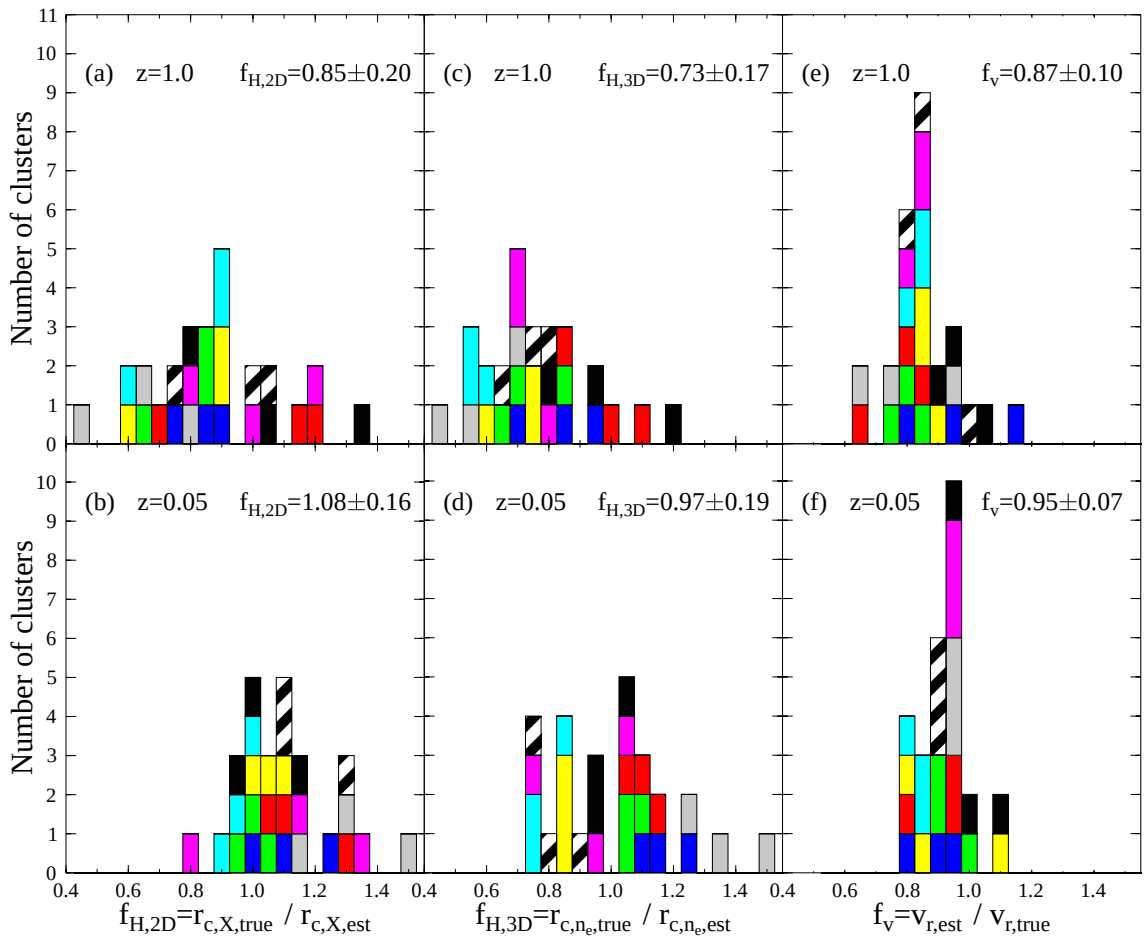

Figure 3: Distribution of the estimated H_0 and v from 9 simulated clusters at $z = 0.05$ and $z = 1.0$ viewed from three different line-of-sight directions. Different patterns of the histogram correspond to different clusters. (Yoshikawa, Itoh + YS 1998)

⋆ Inhomogeneous structure of RXJ 1347 ($z = 0.45$)

Cluster structure may not be so simple as you wish !

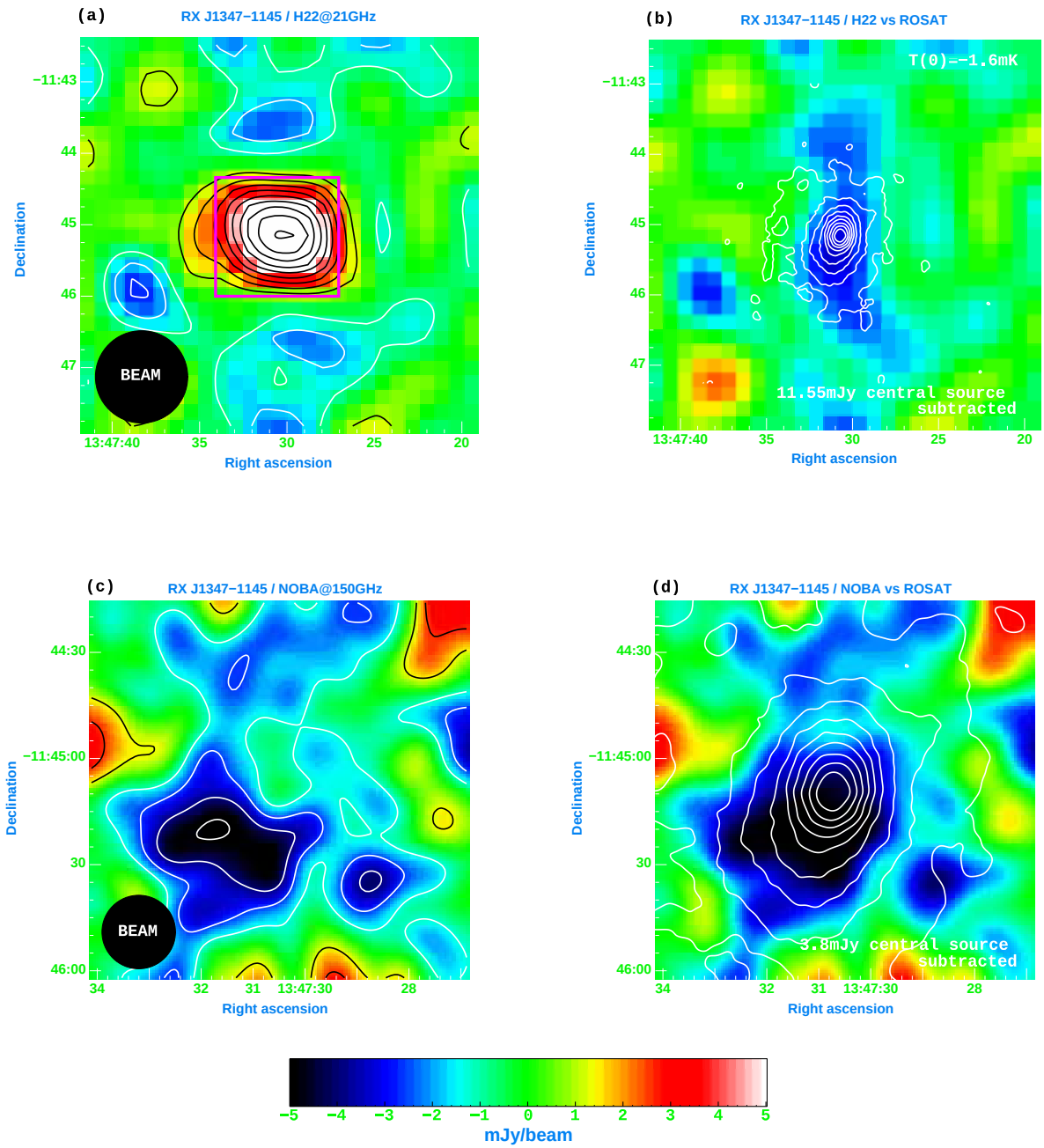

Figure 4: The SZ maps of RX J1347–1145. (a) the 21 GHz map: $6' \times 6'$ ($2.4\ h_{50}^{-1}$ Mpc $\times$ $2.4\ h_{50}^{-1}$ Mpc). (b) the 21 GHz map after subtracting the central point source. (c) the 150 GHz map: $1'9 \times 1'9$ ($0.75\ h_{50}^{-1}$ Mpc $\times$ $0.75\ h_{50}^{-1}$ Mpc). (d) the 150 GHz map after subtracting the central point source (assuming the flux of 3.8 mJy) overlaid with the X-ray contours. (Komatsu et al. 2000)

4 Cluster abundances

X-ray Temperature function:

Henry & Arnaud (1991), White, Efstathiou, & Frenk (1993), Kitayama + YS (1996), Viana & Liddle (1996), Eke, Cole, & Frenk (1996)

X-ray luminosity function and log N - log S:

Evrard & Henry (1991), Blanchard & Silk (1991), Barbosa, Bartlett & Blanchard (1996), Ebeling et al. (1997), Rosati & Della Ceca (1997), Oukbir, Bartlett, & Blanchard (1996), Kitayama + YS (1997)

Mass function

Bahcall & Cen (1993), Ueda, Itoh + YS (1993)

Velocity function:

Shimasaku (1993), Ueda, Shimasaku, Suginohara + YS (1994)

⋆ crucial assumption

one-to-one correspondence between a virialized halo and an X-ray cluster. The former is defined through a spherical collapse model à la Press-Schechter, or selected from simulations with friend-of-friend or spherical overdensity algorithms.

a reasonable working hypothesis, but needs justification if adopted for quantitative discussion

4.1 Predicting cluster abundances

model for halo mass function: $n_{\rm M}(M,z)$

Press & Schechter (1974), Sheth & Tormen (1999), Sheth, Mo & Tormen (1999), Jenkins et al. (2000)

halo mass → gas temperature

$$kT(z) = \gamma \frac{\mu m_p G M}{3 r_{\rm vir}(M,z)} \qquad (\gamma = 1.2)$$

gas temperature → luminosity

$$L_{\rm bol}(z) = L_{44} \left(\frac{T(z)}{6{\rm keV}}\right)^{\alpha} (1+z)^{\zeta}\, 10^{44} h^{-2}\ {\rm erg\ sec}^{-1}$$

($L_{44} = 2.9$, $\alpha = 3.4$, and $\zeta = 0$; David et al. 1993)

band correction: $f(T, E_a, E_b)$

$$L_{\rm band} = L_{\rm bol}(z) \times f[T, E_a(1+z), E_b(1+z)]$$

Observed band-limited X-ray flux

$$S_0[E_a, E_b] = \frac{L_{\rm band}[E_a(1+z), E_b(1+z)]}{4\pi d_L^2(z)}$$

Number of clusters per unit solid angle

$$\begin{aligned} N(>S) &= \int_0^\infty dz\ d_A^2(z) c \left|\frac{dt}{dz}\right| \\ &\times \int_S^\infty dS_0\ (1+z)^3 n_M(M,z) \\ &\times (dM/dT)(dT/dL_{\rm band})(dL_{\rm band}/dS_0) \end{aligned}$$

⋆ X-ray Log N - Log S in CDM models

some models are consistent with observations.

strong Ω_0 and σ_8 dependence.

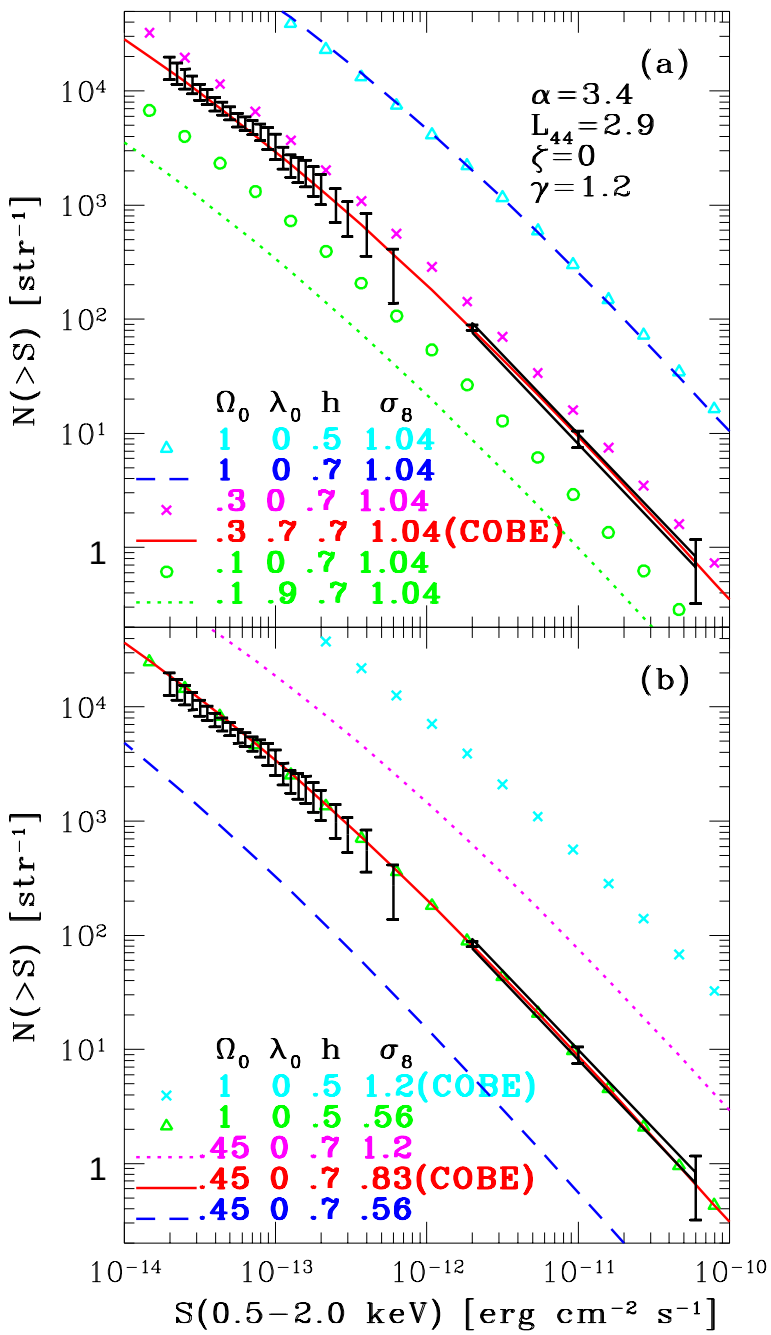

Figure 5: (a) $\sigma_8 = 1.04$, (b) $\Omega_0 = 1$ and $\Omega_0 = 0.45$ models. (Kitayama + YS 1997)

⋆ Limits on Ω_0 and σ_8 in CDM models

$\sigma_8 \sim 0.55\Omega_0^{-0.55}$. Combined with COBE,

$(\Omega_0, \lambda_0, \sigma_8) = (0.3, 0.7, 1.0), (0.45, 0.0, 0.85)$

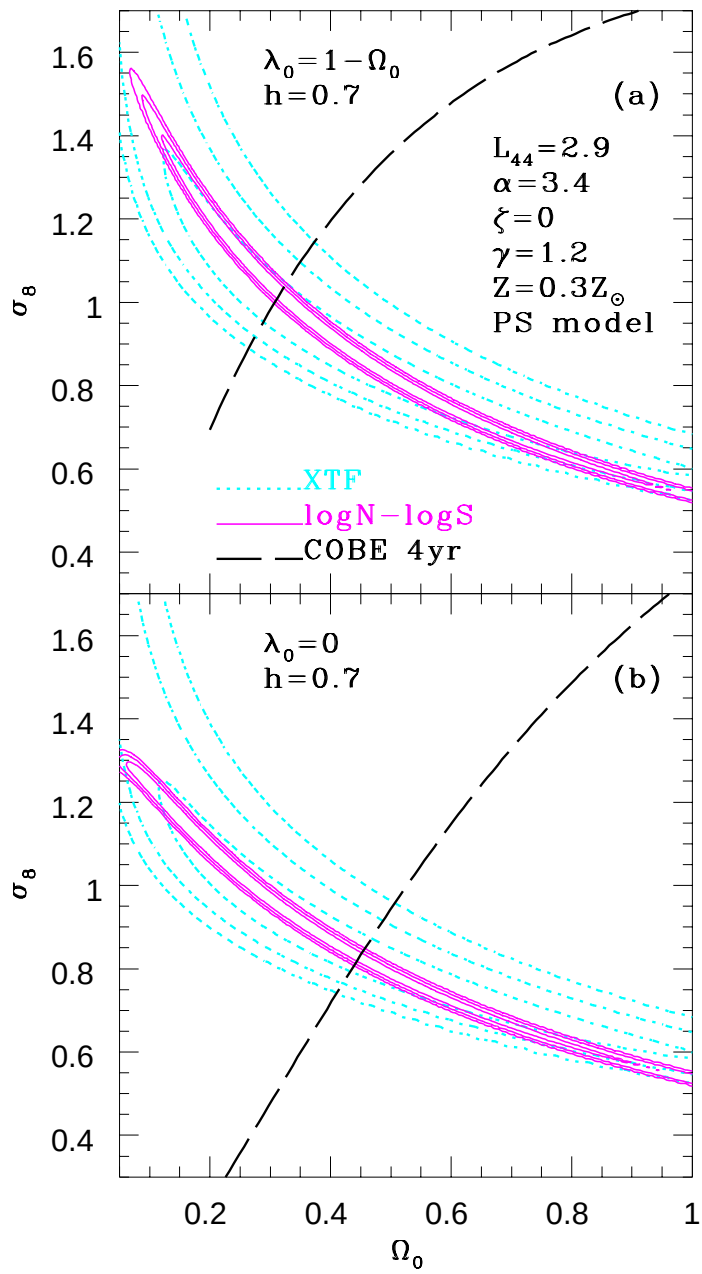

Figure 6: $n = 1$, $h = 0.7$ with (a) $\lambda_0 = 1 - \Omega_0$, and (b) $\lambda_0 = 0$. X-ray cluster Log N - Log S (solid) and XTF (dotted) are plotted as contours at $1\sigma(68\%)$, $2\sigma(95\%)$ and $3\sigma(99.7\%)$ confidence levels. (Kitayama + YS 1997)

⋆ Systematic effects ($\lambda_0 = 1 - \Omega_0$ CDM models)

Model uncertainties yield $\pm 20\%$ systematic errors in σ_8

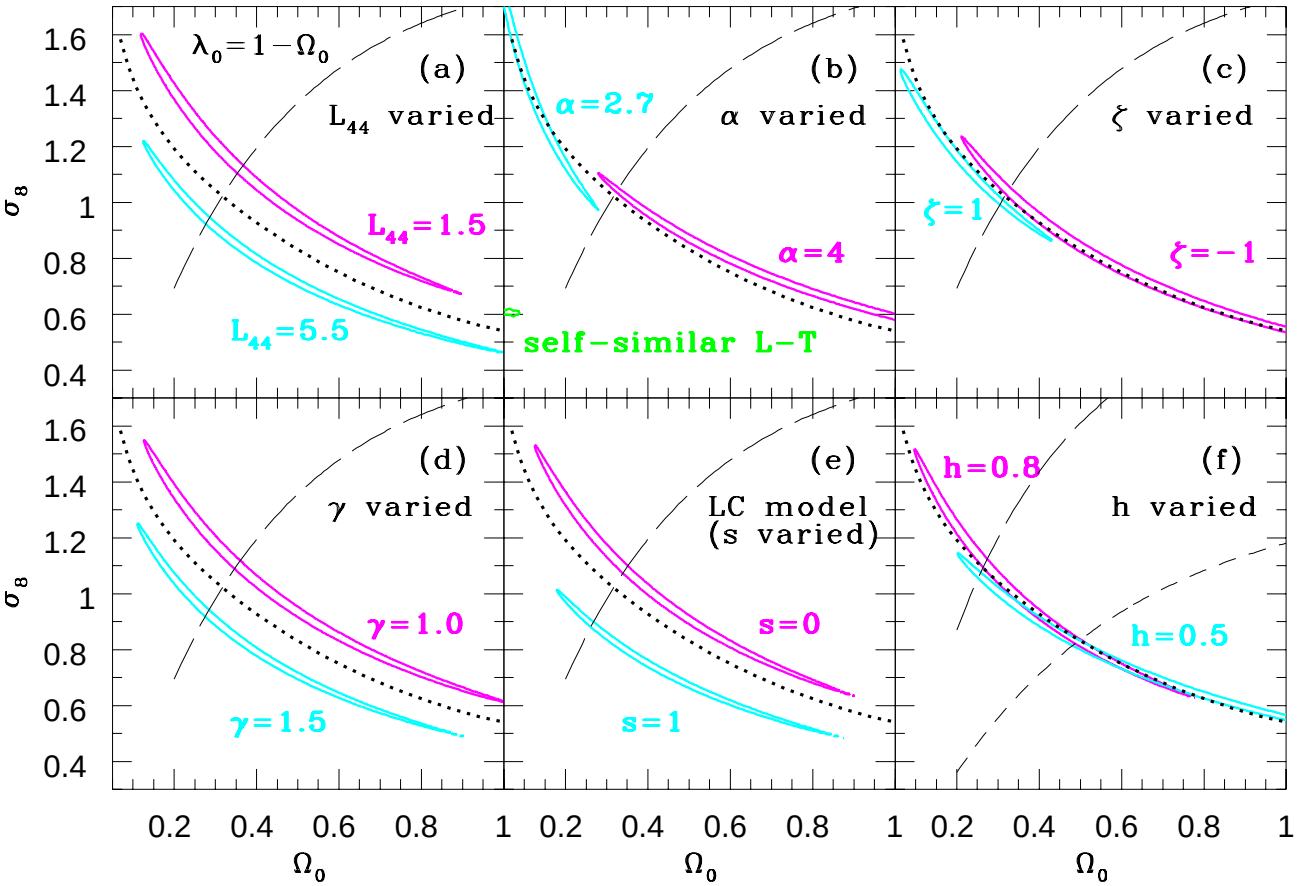

Figure 7: (a) L_{44}, (b) α, (c) ζ, (d) γ, (e) s, and (f) h. Except for the parameters varied in each panel, our canonical set of parameters ($L_{44} = 2.9$, $\alpha = 3.4$, $\zeta = 0$, $\gamma = 1.2$, $h = 0.7$). Dotted and dashed lines represent our best-fit for the canonical parameter set and the *COBE* 4 year results, respectively.

(Kitayama + YS 1997)

4.2 Breaking the degeneracy

Many cosmological models are known to be more or less successful in reproducing the structure at redshift $z \sim 0$ *by construction*.

$\Downarrow$

This is because the models have still several degrees of freedom or *cosmological parameters* which can be appropriately *adjusted* to the observations at $z \sim 0$ (Ω_0, σ_8, h, λ_0, $b(r, z)$).

How to break the degeneracy among the viable models ?

$\Downarrow$

Wider: increase the statistics from wide-field surveys (SDSS, PLANCK, ...)

Deeper: observe clusters at higher redshifts

Different bands: mm and submm bands in addition to the optical and X-ray bands.

(e.g., Eke, Cole, & Frenk 1996;
Barbosa, Bartlett, Blanchard, & Oukbir 1996;
Fan, Bahcall, & Cen 1997;
Kitayama, Sasaki + YS 1998)

⋆ Breaking the degeneracy of number counts

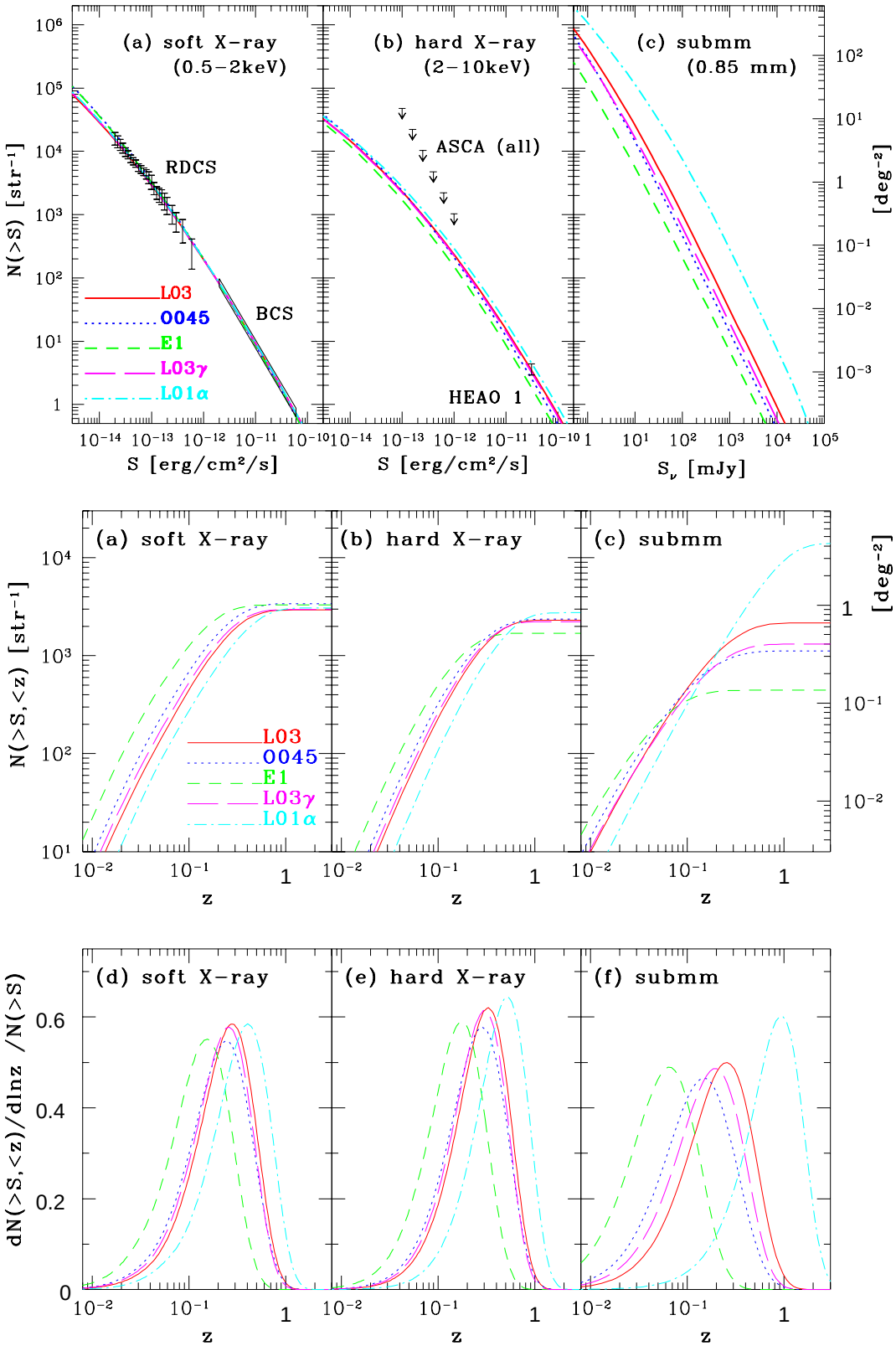

Figure 8: (a) soft X-ray (0.5-2.0 keV), (b) hard X-ray (2-10 keV), and (c) submm (0.85 mm) bands. *Upper:* Different bands, *Lower:* different redshifts. Kitayama, Sasaki + YS (1998)

⋆ Predicted contours

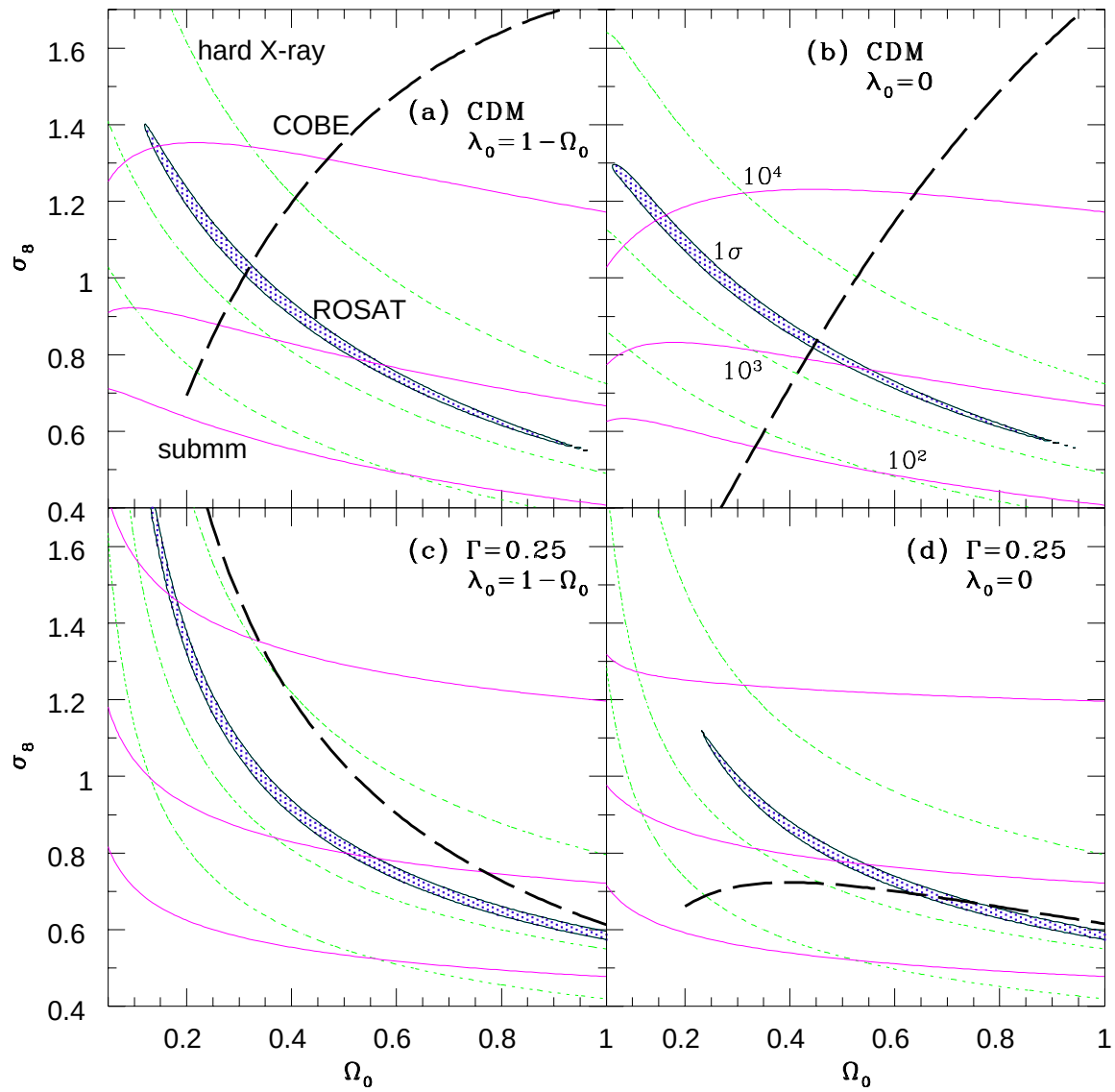

Figure 9: Shaded regions represent the 1σ significance contours derived in KS97 from the soft X-ray (0.5-2 keV) Log N - Log S. Dotted and solid lines indicate the predicted contours of the number of clusters in the hard X-ray (2-10 keV) band at $S = 10^{-13}$ erg cm^{-2} s^{-1} in the submm (0.85 mm) band at $S_\nu = 10^2$mJy. Kitayama, Sasaki + YS (1998)

5 Spatial correlation

Strong spatial clustering of clusters relative to galaxies (Bahcall & Soneira 1983; Klypin & Kopylov 1983)
→ inspired the idea of biasing (Kaiser 1984)
→ regularity in the clustering amplitude (Bahcall 1988; Bahcall & West 1992)

⋆ Two-point correlation functions of X-ray selected clusters (Borgani et al. 1999; Moscardini et al. 2000; YS, Yamamoto, Kitayama, & Jing 2000)

Two-point correlation functions of clusters on the light-cone brighter than the X-ray flux-limit $S_{\rm lim}$

$$\xi^{\rm LC}_{\rm X-cl}(R;>S_{\rm lim}) = \frac{\int_{z_{\rm max}}^{z_{\rm min}} dz \frac{dV_{\rm c}}{dz}\, n_0^2(z) \xi^{\rm S}_{\rm cl}(R, z(r); > S_{\rm lim})}{\int_{z_{\rm max}}^{z_{\rm min}} dz \frac{dV_{\rm c}}{dz}\, n_0^2(z)}$$

bias parameter $b(z, M)$ analytic model (Mo & White 1996) + N-body simulations (Jing 1998)

selection function halo mass function from the Press-Schechter theory + $L_{\rm X}(M, z)$, $T_{\rm X}(M, z)$, $S_{\rm X}(M, z)$

redshift-space distortion Kaiser (1987), Peacock & Dodds (1996), Magira, Jing + YS (2000)

cosmological light-cone effect Yamamoto + YS (1999), Yamamoto, Nishioka + YS (1999), Hamana, Colombi + YS (2000)

⋆ Model predictions for X-ray cluster correlation functions with redshift-space distortion and light-cone effects

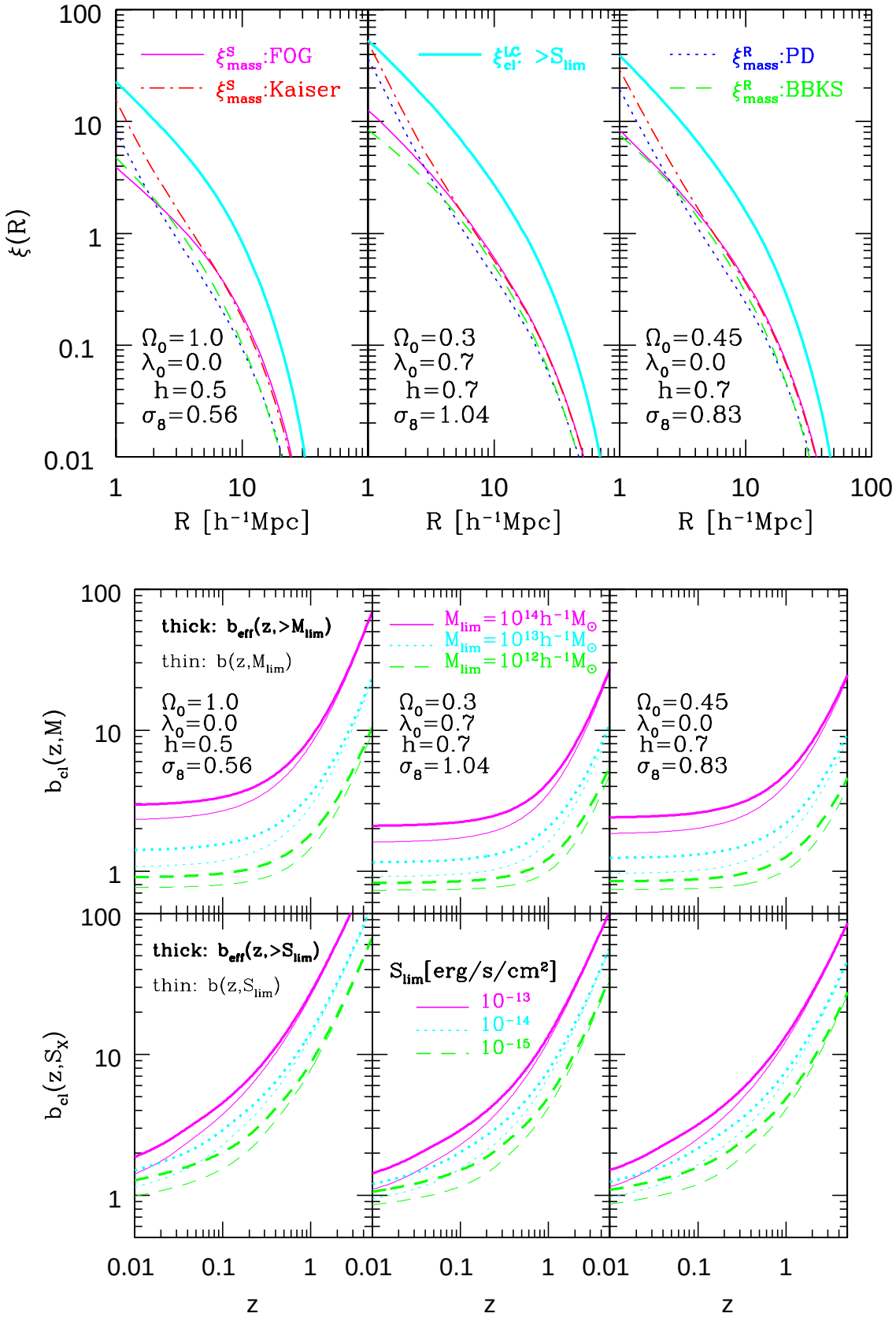

Figure 10: (YS, Yamamoto, Kitayama & Jing 2000)

⋆ The redshift-distortion and light-cone effects on the two-point correlation functions in CDM

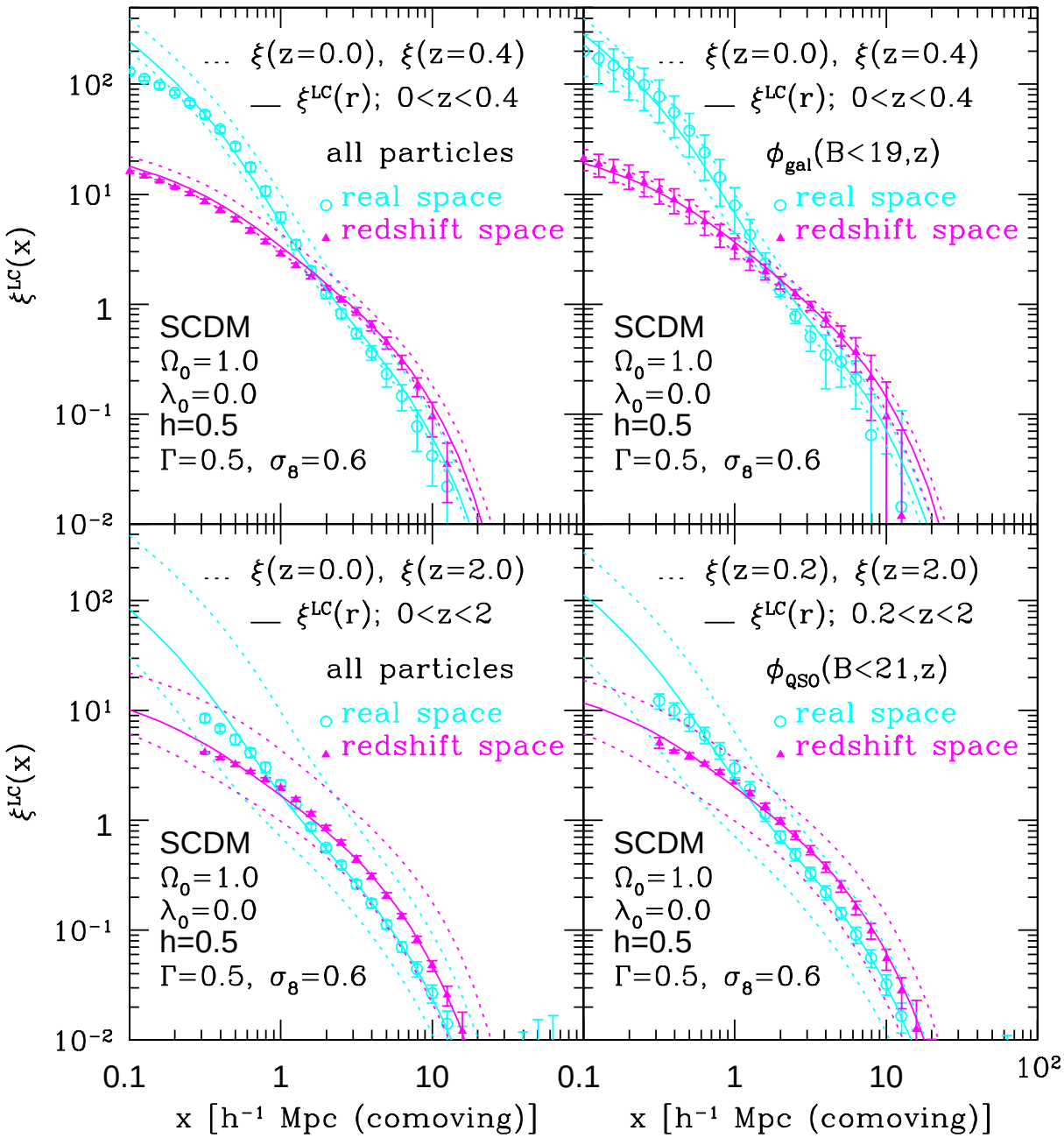

Figure 11: *Upper:* $0 < z < 0.4$, *Lower:* $0 < z < 2.0$. *Left:* without selection functions, *Lower:* with selection functions. (Hamana, Colombi + YS 2000)

⋆ Ω_0-dependence of X-ray cluster correlation lengths

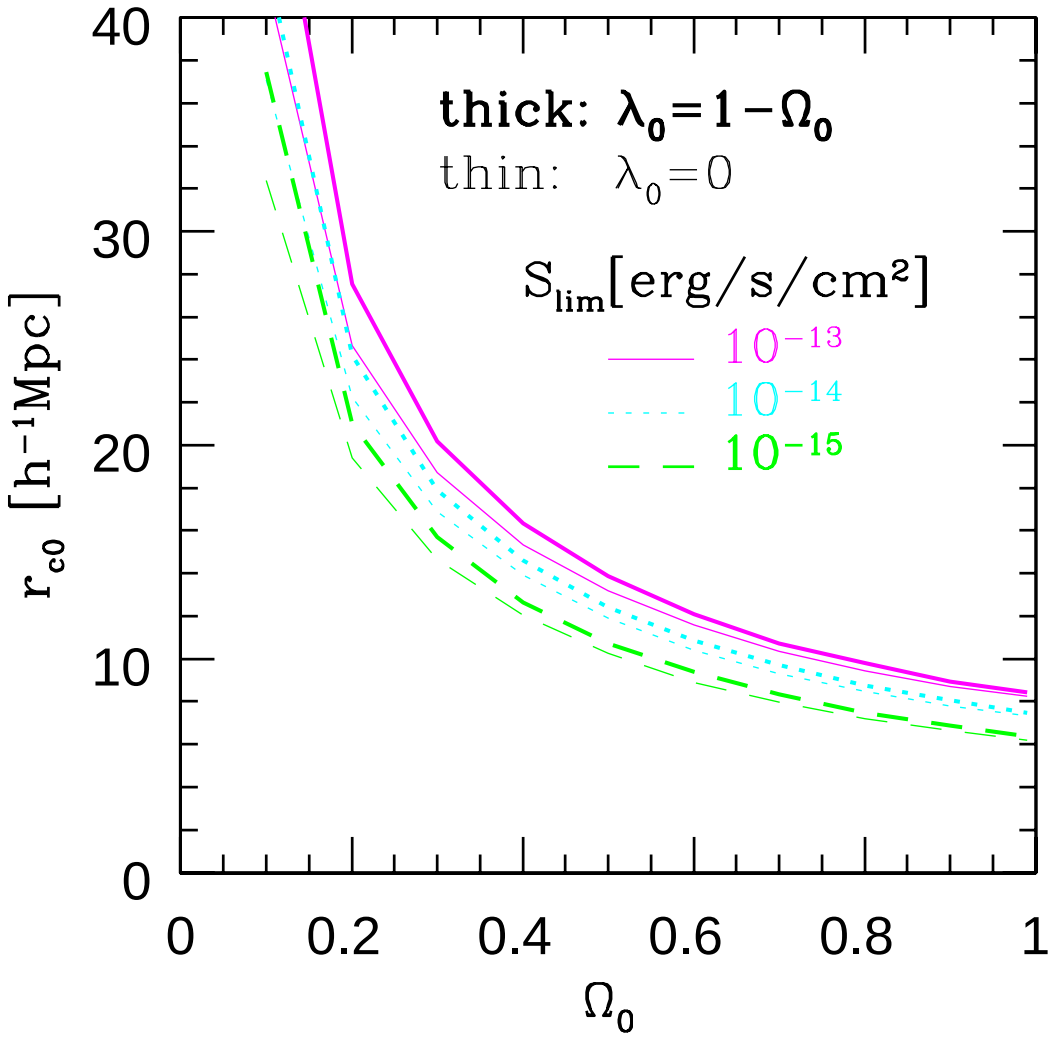

Figure 12: The X-ray flux-limit $S_{\rm lim}$ is 10^{-13} (solid lines), 10^{-14} (dotted) and 10^{-15}erg/s/cm^2 (dashed). For each $S_{\rm lim}$, we plot the case of $\lambda_0 = 1 - \Omega_0$ in thick lines, and $\lambda_0 = 0$ in thin lines. Fluctuation amplitudes are normalized by the cluster abundance. (YS, Yamamoto, Kitayama & Jing 2000)

⋆ Nonlinear and stochastic biasing of halos

In reality, halo biasing may be very complicated

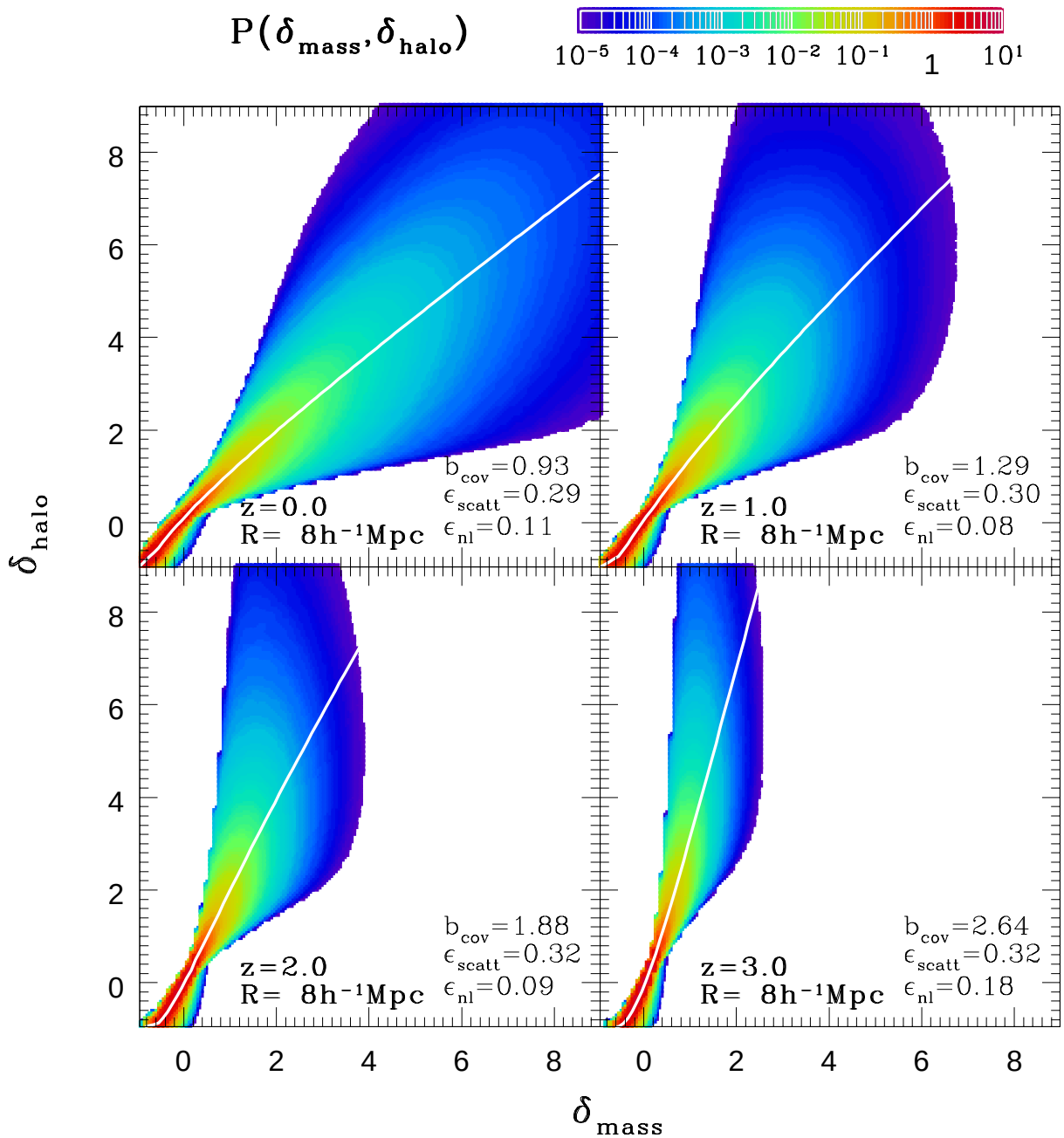

Figure 13: $10^{11}h^{-1}M_\odot < M < 10^{13}h^{-1}M_\odot$ in LCDM model. *Upper-left:* $z = 0$; *Upper-right:* $z = 1$; *Lower-left:* $z = 2$; *Lower-right:* $z = 3$. Taruya + YS (2000)

6 Universal density profile

Original question: Are the observed flat rotation curves of galaxies ($\rho \propto r^{-2}$) consistent with dark matter halo profile in the hierarchical clustering picture ?

Hoffman & Shaham (1985) predicted $\rho \propto r^{-3(3+n)/(4+n)}$ in the outer region on the basis of the peak + secondary infall argument ($n \equiv d\ln P(k)/d\ln k$).

Quinn, Salmon & Zurek (1986) confirmed the Hoffman & Shaham profile for scale-free models using N-body simulations.

Frenk, White, Davis & Efstathiou (1988) reproduced the flat rotation curves from N-body simulations in CDM models.

Suginohara + YS (1992) showed that the profile is sensitive to the group-finding algorithm, and it is clear if CDM models account for the flat rotation curves.

Navarro, Frenk & White (1996, 1997) claimed the universal density profile: $\rho_{\rm NFW}(r) \propto (r/r_s)^{-1}(1+r/r_s)^{-2}$ from higher resolution simulations.

Fukushige & Makino (1997) claimed that the inner profile is $r^{-1.5\sim-2}$ using GRAPE rather than r^{-1}.

Evans & Collett (1997) found a steady-state, self-consistent cusped solution to the collisional Boltzmann equation corresponding to $\rho \propto r^{-4/3}$.

Syer& White (1998) predicted $\rho \propto r^{-3(3+n)/(5+n)}$ analytically.

Moore et al. (1998) confirmed that the inner profile is steeper and the universal profile should be $\rho \propto (r/r_s)^{-1.5}[1+(r/r_s)^{1.5}]^{-1}$

Jing + YS (2000) found the mass-dependence of the profile; the profile is not strictly universal.

6.1 Numerical results

⋆ Universal density profile of dark matter halo (Navarro, Frenk, & White 1997, ApJ, 490, 493)

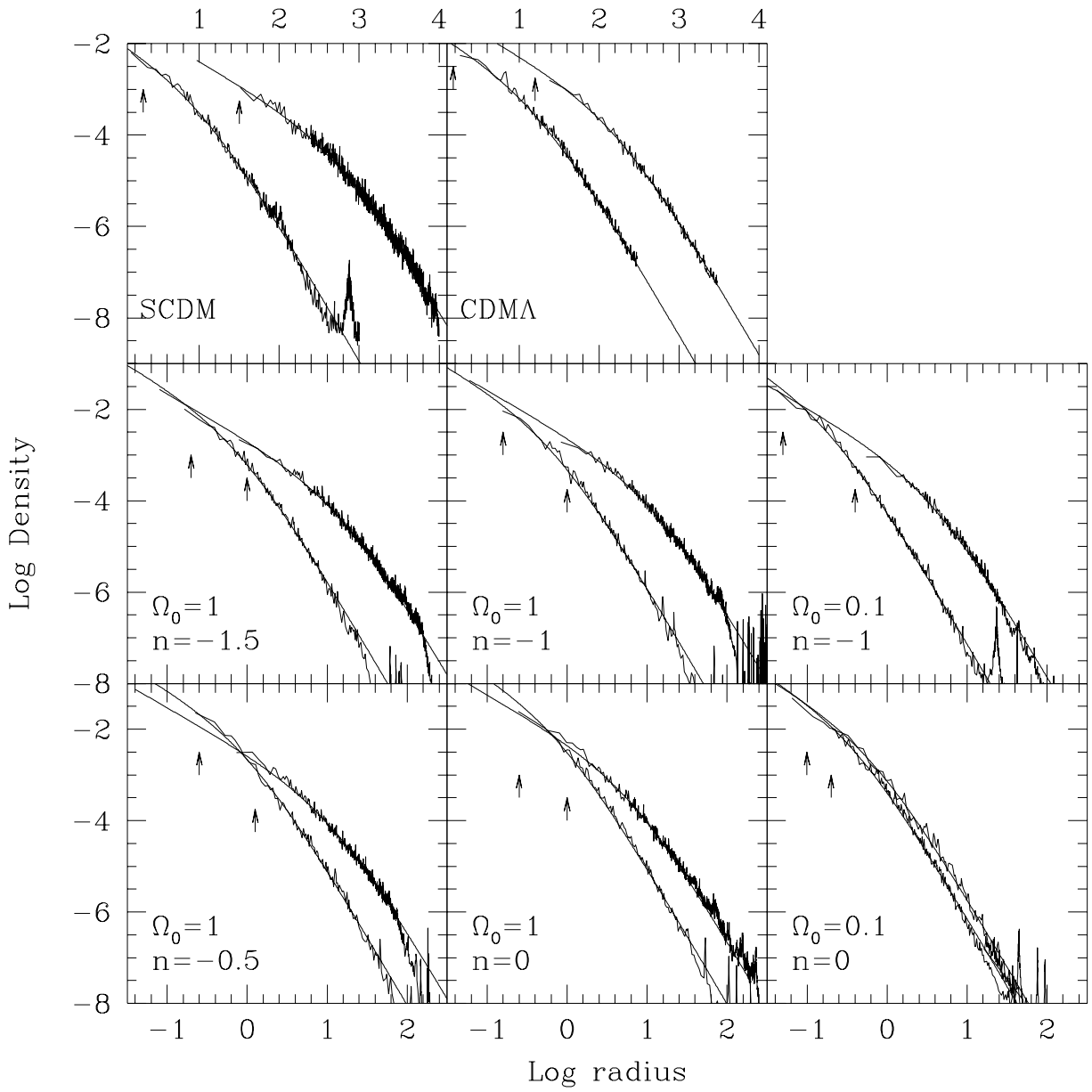

Figure 14: Density profiles of one of the most and one of the least massive halos in each series. The arrows indicate the value of the gravitational softening.

⋆ Higher–resolution simulations using GRAPE (Fukushige & Makino 1997, ApJL, 477, L9)

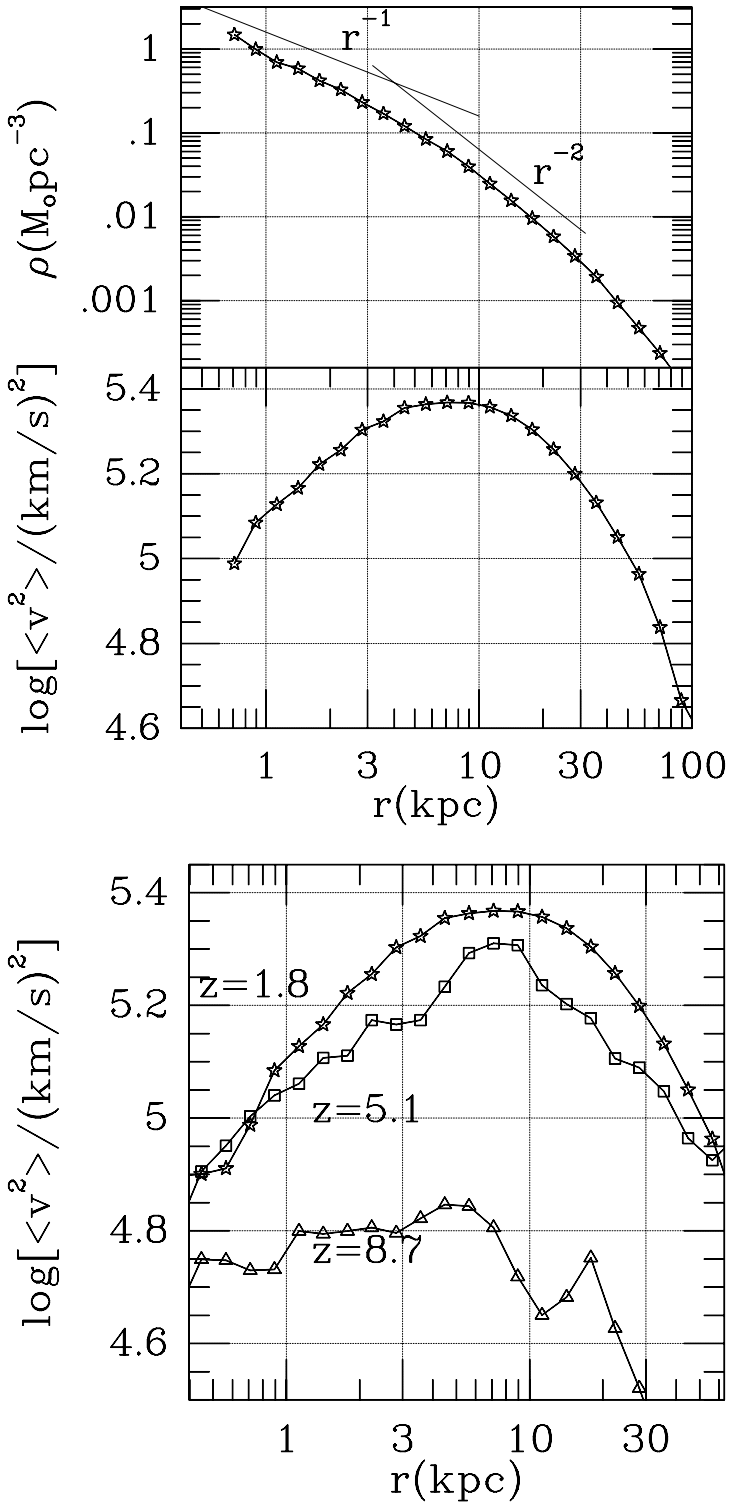

Figure 15: Density and velocity dispersion profiles.

⋆ The profiles of simulations are converged ?
(Moore et al. 1998, ApJL, 499, L5)

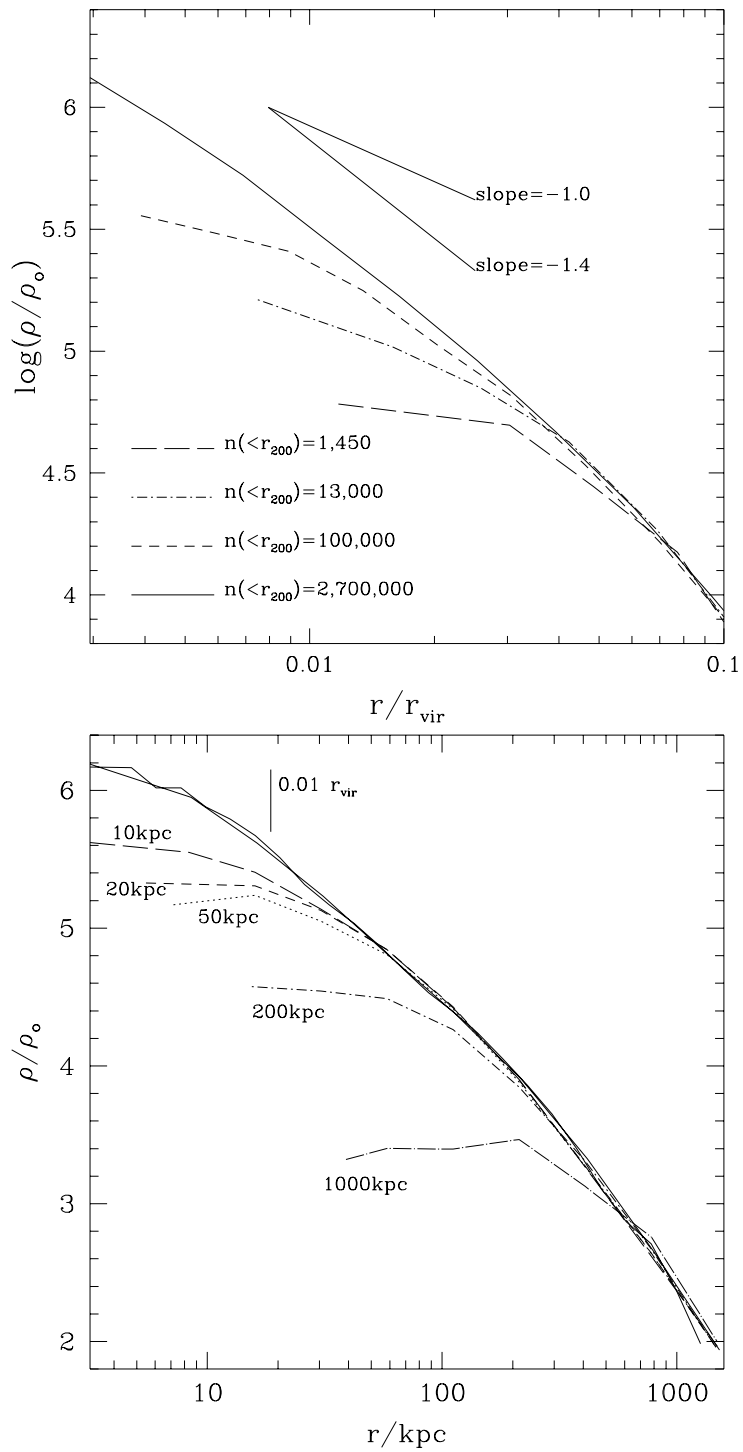

Figure 16: Dependence on the number of simulation particles and on the adopted gravitational softening length.

⋆ Projected snapshots of simulated dark matter halos.
(Jing + YS 2000, ApJL, 529, L69)

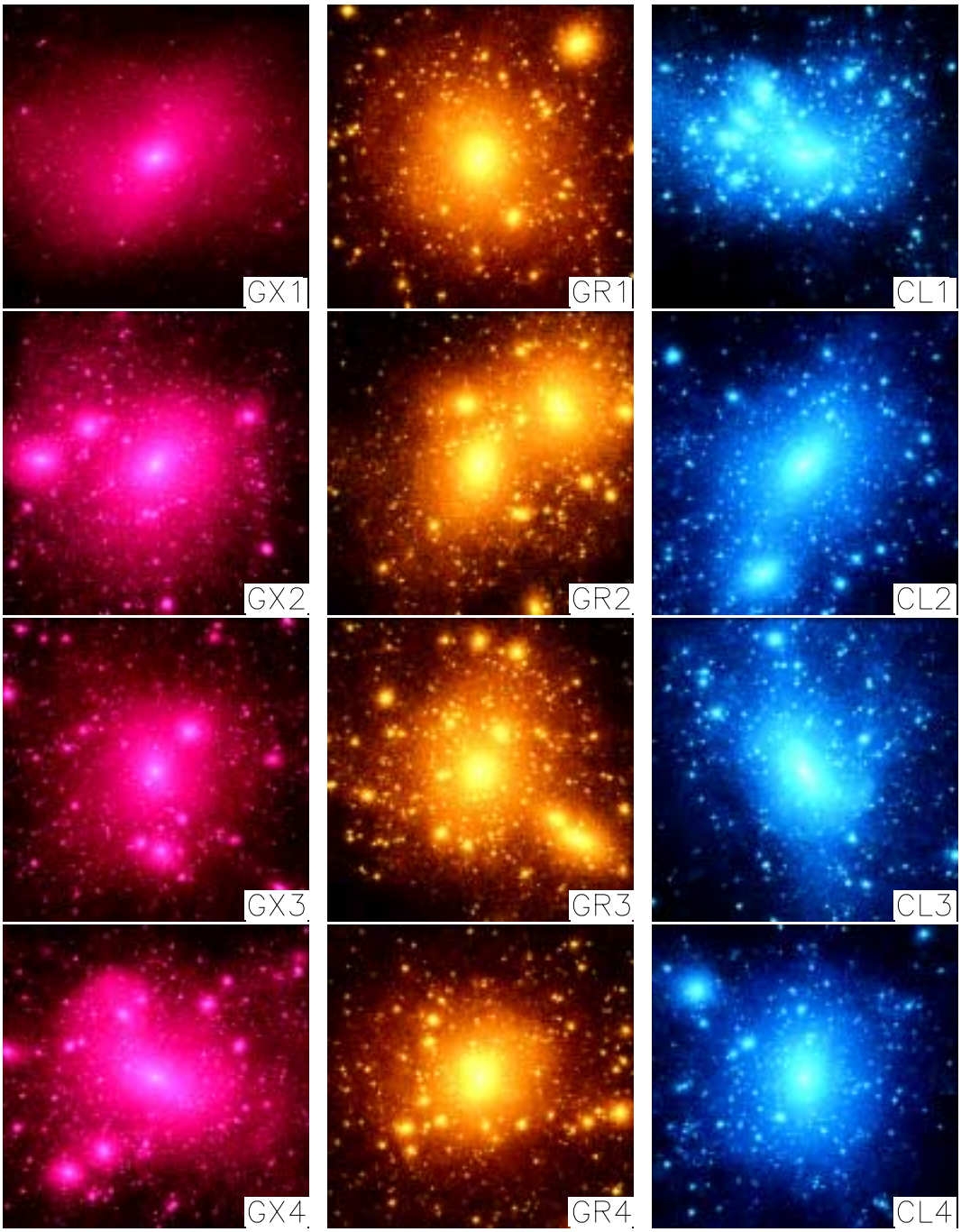

Figure 17: Snapshots of the simulated halos at $z = 0$. Left, middle and right panels display the halos of galaxy, group and cluster masses, respectively (see Table 1). The size of each panel corresponds to $2r_{\rm vir}$ of each halo.

⋆ Profiles of simulated dark matter halos.

(Jing + YS 2000, ApJL, 529, L69)

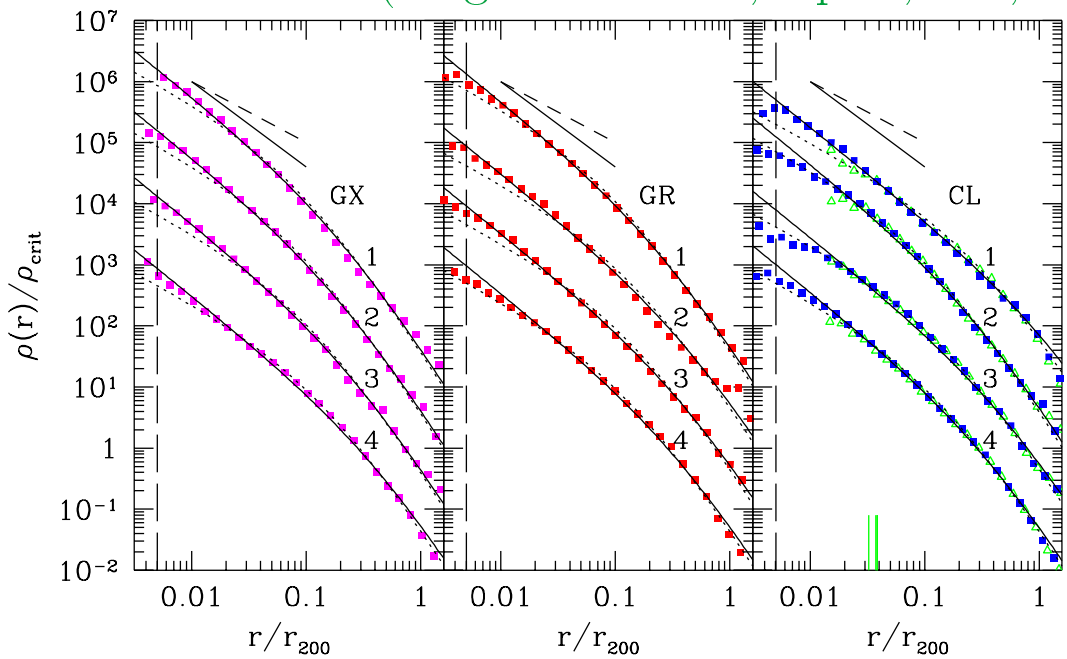

Figure 18: Spherically-averaged radial density profiles of the simulated halos of galaxy (*left*), group (*middle*), and cluster (*right*) masses. The solid and dotted curves represent fits of $\beta = 1.5$ and $\beta = 1$ respectively

⋆ Inner slope vs. halo mass

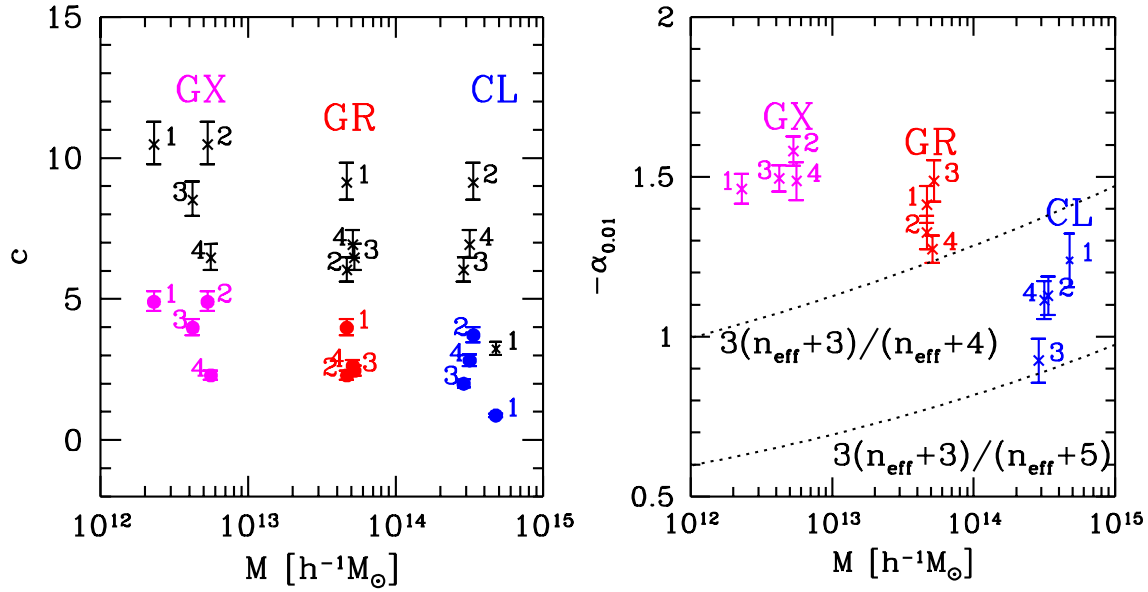

Figure 19: *Left panel:* the concentration parameters for each halo for the $\beta = 1.5$ form (filled circles) and for the NFW form (crosses). *Right panel:* Power-law index of the inner region ($0.007 < r/r_{200} < 0.02$) as a function of the halo mass. The upper and lower dotted curves indicate the predictions of Hoffman & Shaham (1985) and Syer & White (1996), respectively.

6.2 Observational confrontation

⋆ Gas density profile from the universal dark halo

The analytic solution for gas density (NFW mass profile + isothermal) turns out to be very well approximated by the conventional isothermal β-model:

$$\rho(r) \propto [1 + (r/r_c)^2]^{-3\beta/2}$$

with $\beta = 0.9(8\pi G\mu m_p \delta_c \rho_{c0} r_s^2/27kT)$ and $r_c = 0.22 r_s$.

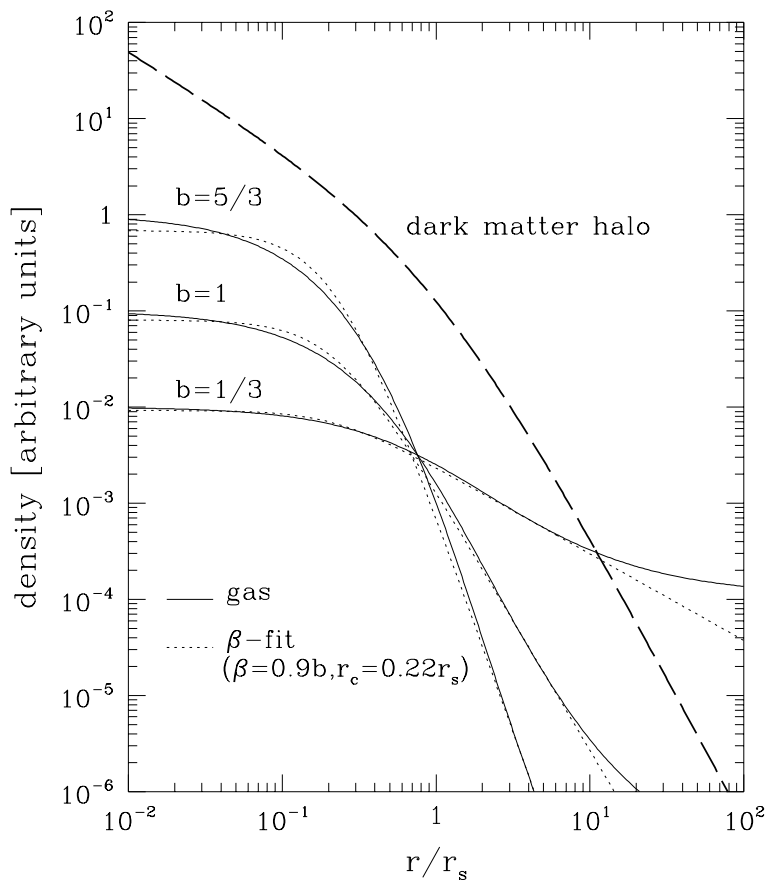

Figure 20: Density profiles of gas (solid lines), the universal dark matter halo (dashed line), and The best-fit β-models with $\beta = 0.9b$ and $r_c = 0.22r_s$ (dotted lines). (Makino, Sasaki +YS, ApJ, 1998, 497, 555)

⋆ Predicted core radii from the universal dark halo.
much smaller than the observed values for X-ray clusters

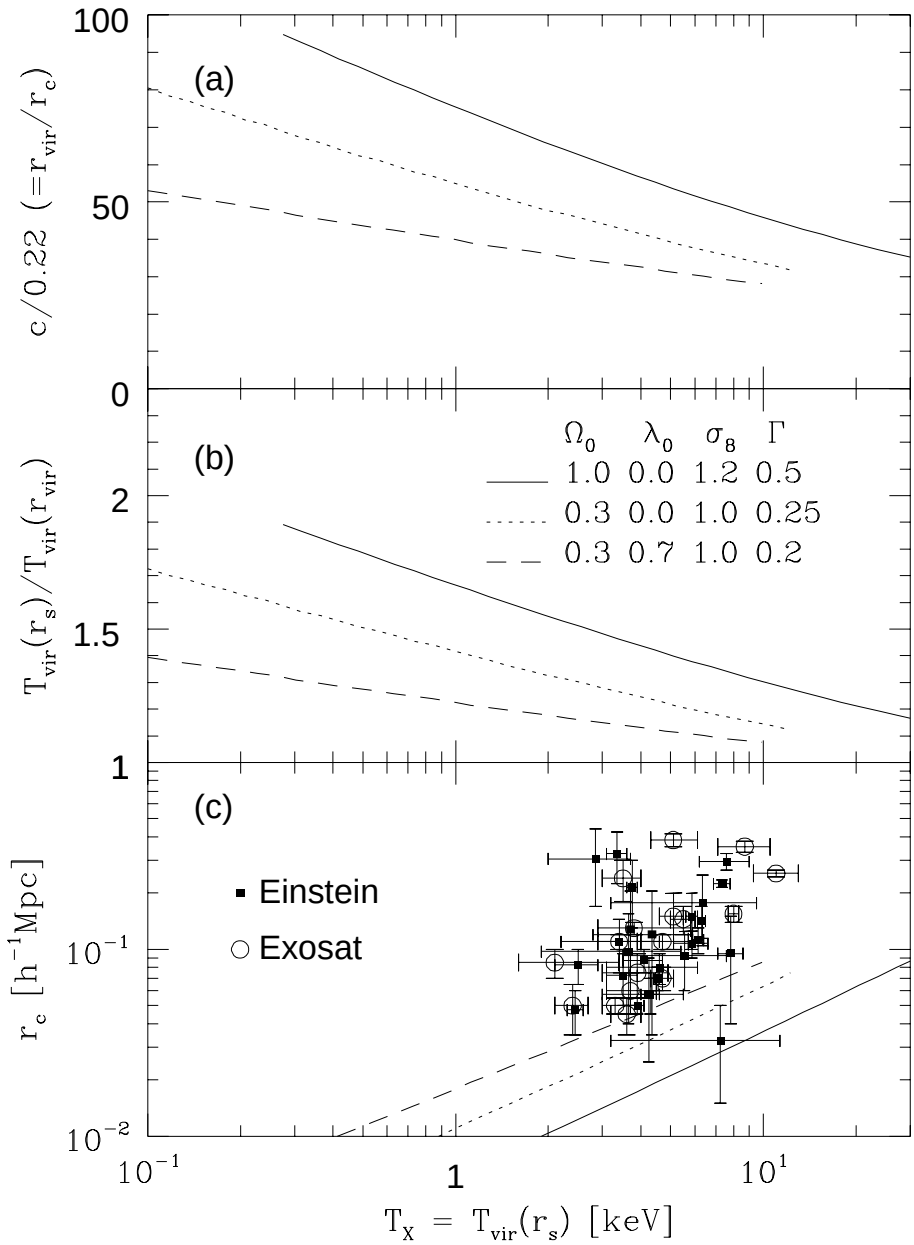

Figure 21: Solid, dotted and dashed lines indicate SCDM ($\Omega_0 = 1$, $\lambda_0 = 0$, $\Gamma = 0.5$, $\sigma_8 = 1.2$), OCDM ($\Omega_0 = 0.3$, $\lambda_0 = 0$, $\Gamma = 0.25$, $\sigma_8 = 1.0$), and LCDM ($\Omega_0 = 0.3$, $\lambda_0 = 0.7$, $\Gamma = 0.2$, $\sigma_8 = 1.0$). (Makino, Sasaki +YS 1998)

⋆ $c - M_{\rm vir}$, $\delta_{\rm c} - M_{\rm vir}$ relations from 63 ROSAT clusters.
CDM + NFW predictions differ from X-ray data

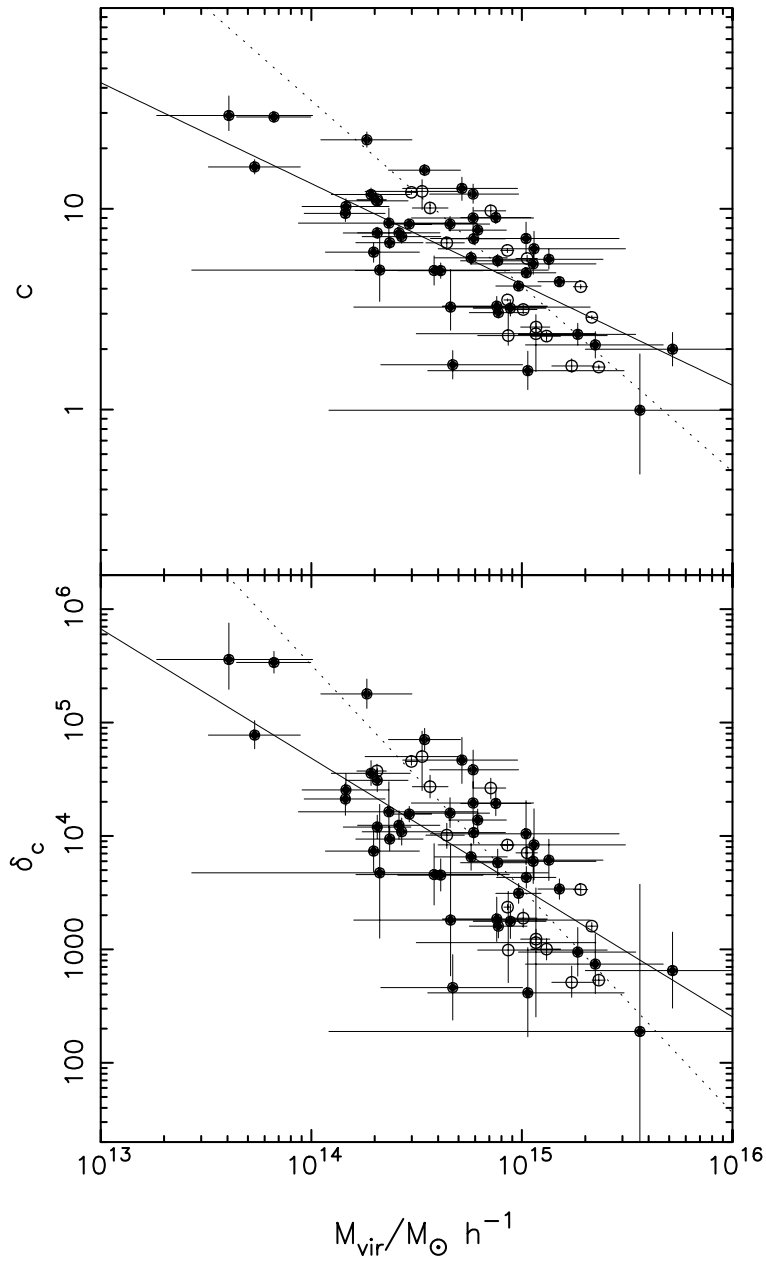

Figure 22: $\Omega_M = 0.3$ and $\Omega_\Lambda = 0.7$ are assumed. The MME and EF clusters are represented by the filled and open circles, respectively. (Wu & Xue, ApJL 2000, 529, L5)

6.3 Relation to nonlinear mass power spectrum

⋆ Recovering $P_{\rm DM}(k)$ from universal profiles + halo bias

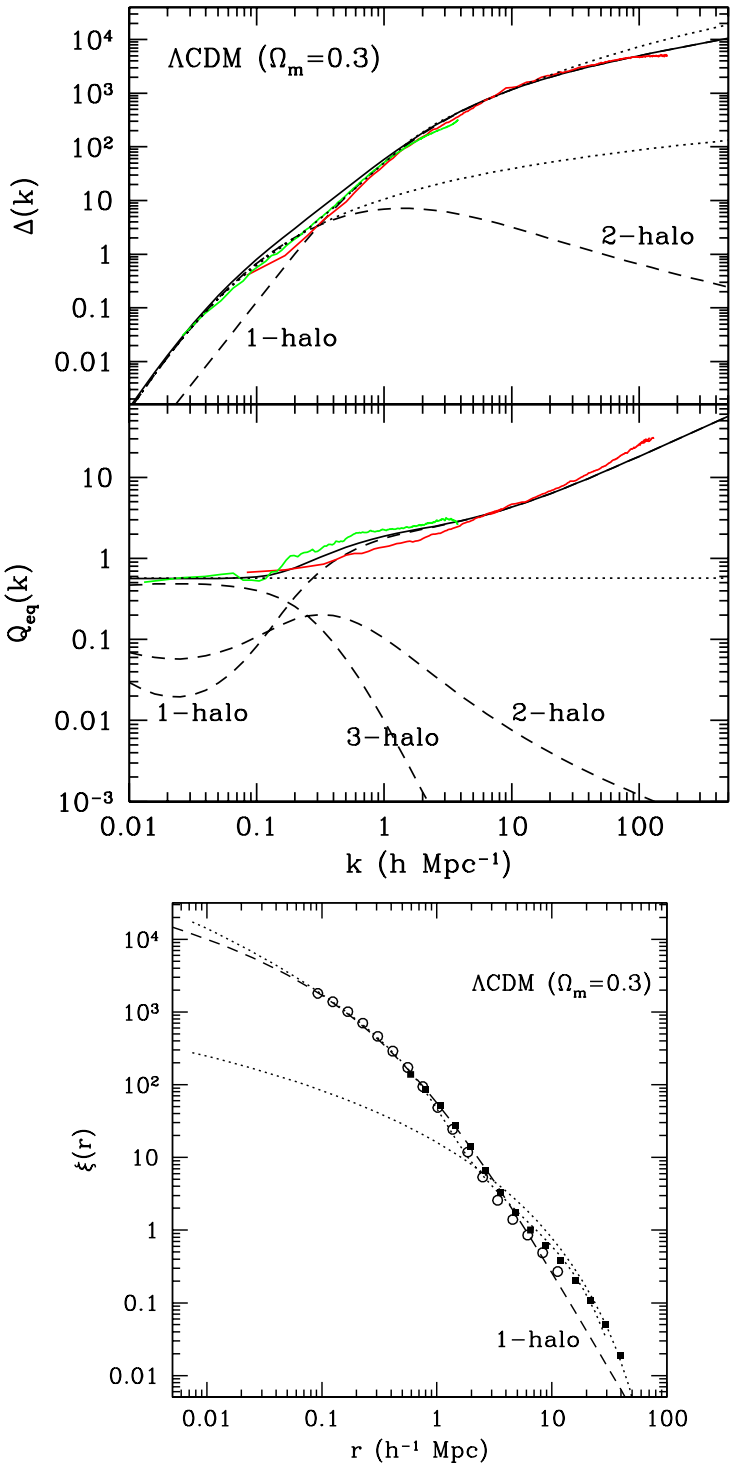

Figure 23: Ma & Fry (2000); see also Seljak (2000)

7 Summary and conclusions

SZ effect as a distance indicator:

- reasonably useful, but not quite
- more realistic (non-spherical, inhomogeneous ...) effects should be included

(→ talks by J.Bartlett, J.Carlstrom, Y.Rephaeli ...)

Cluster abundances:

- very successful constraints on σ_8–Ω_0
- will be significantly improved with multi-band and/or high-z observational data
- Press-Schechter like objects = objects identified in simulations = observed optical/X-ray clusters are not guaranteed !

(→ talks by A.Blanchard, S.Borgani, M.Dickinson ...)

Spatial correlation:

- important clues to clustering on large scales
- more reliable models for halo biasing, light-cone and distortion effects are essential

(→ talks by H.Böhringer, P.Schuecker, ...)

Universal density profile:

- surprising regularity in the density profile of virialized objects
- another route to understanding nonlinear gravitational clustering of dark matter
- inconsistent with observations ?
  → *beyond* the universal density profile ?
  or → *beyond* CDM (WDM, SIDM, ...) ?

(→ talks by B.Moore, A.Evrard, ...)